Rotational band structure in ^{75}Se

T. D. Johnson, T. Glasmacher, J. W. Holcomb, P. C. Womble, and S. L. Tabor

Department of Physics, Florida State University, Tallahassee, Florida 32306

W. Nazarewicz*

Department of Physics, Florida State University, Tallahassee, Florida 32306
and Joint Institute for Heavy Ion Research, Holifield Heavy Ion Research Facility, Oak Ridge, Tennessee 37831
(Received 31 January 1992)

The high-spin states of ^{75}Se have been investigated using the ^{59}Co(^{19}F,$2pn$) reaction at 55 MeV. The positive-parity band has been extended to $I^\pi = \frac{29}{2}^+$ and the unfavored signature has been identified. The negative-parity band has been extended to $I^\pi = \frac{19}{2}^-$ and band crossings were observed for the first time in both bands. Eleven new lifetimes were measured using the Doppler-shift attenuation method which allowed for extraction of transition strengths and transition quadrupole moments. The $B(M1)$ strengths exhibit a staggering dependent on the signature splitting. Calculations based on the Woods-Saxon-Bogolyubov cranking model explain the signature-dependent alignment process in the $g_{9/2}$ bands and predict signature inversion in all bands at high rotational frequencies. It is argued that the data are consistent with the transition from triaxial shapes with $\gamma \sim -30°$, characteristic of one-quasiparticle configurations, to triaxial shapes with $\gamma \sim 30°$, characteristic of a three-quasiparticle configuration containing one aligned pair of $g_{9/2}$ protons.

PACS number(s): 21.10.Re 25.70.−z 27.50.+e

I. INTRODUCTION

The light Se isotopes provide a rich testing ground for examining effects of single-particle levels and competing shapes on collectively rotating structures. The Ge-Kr isotopes with $A \sim 70$ are also one of the best examples of the ground-state nuclear shape isomerism; see, e.g., reviews [1–4]. Calculations suggest an interpretation in terms of two competing configurations: one at an oblate shape, and one at a prolate shape. Nearly oblate ground states are predicted for the Ge and Se isotopes, while for the Kr isotopes the prolate configuration lies lower in energy. Because of the mutual interaction (of the order of a few hundred keV) the prolate and oblate bands are strongly disturbed in the crossing region.

The coexistence of prolate and oblate configurations around ^{72}Se has recently been supported by the high-spin spectroscopy of neighboring odd-A isotopes. For ^{69,71}Se Wiosna et al. [5] established rotational $g_{9/2}$ bands based on prolate and oblate shapes. The evidence is based on different signature splitting in these bands as well as on the sign of the mixing ratio of interband transitions. Recent studies [6, 7] of ^{73}Se revealed a γ-soft structure with a decoupled $g_{9/2}$ band showing a strong signature dependence in the alignment process. For the $N = 43$ Se isotope, ^{77}Se, two negative-parity bands and a decoupled $g_{9/2}$ band have been observed [8] and interpreted in terms of strongly triaxial shapes [9]. The level scheme of ^{79}Se ($N = 45$) is already vibrationlike [9], indicating

a transition towards spherical shapes when approaching the neutron closure at $N = 50$.

For the even-even Se isotopes the recent experimental data for ^{70,72}Se [10] and ^{74}Se [11, 12] reveal a very regular yrast band above $I = 10\hbar$. Results of calculations [10] indeed suggest that at higher rotational frequencies the prolate, better deformed, configuration becomes yrast, i.e., a shape transition from oblate shapes to prolate shapes is expected.

It is well known that structural properties in the $A \sim 70$ mass region are very sensitive to proton and neutron number. Isotone comparisons are particularly useful, since, as the deformation changes with proton number, the odd neutron can occupy different Nilsson orbitals. The influence of these single-particle states on the core can then be illuminated. For isotones where the neutron occupies the same orbital, as in ^{77}Kr and ^{79}Sr, the role played by that orbital can also be further explored in such comparisons.

The isotones ^{77}Kr and ^{79}Sr have rotational bands based on a $\frac{5}{2}^+$ bandhead originating from the odd neutron occupying the $[422]\frac{5}{2}$ Nilsson orbital. The neighboring isotone ^{75}Se has a ground-state spin of $\frac{5}{2}^+$ and was measured [13], using microwave methods, to have prolate deformation. Historically, this was one of the first nuclei for which the spherical shell model could not explain the so-called anomalous $\frac{5}{2}^+$ ground state. Since then, numerous researchers [14–22] have investigated this nucleus. Some early studies [14, 16] used the β decay of ^{75}Br to populate levels in ^{75}Se. Sanderson [17] used the reaction ^{76}Se(d,t)^{75}Se and interpreted the results using the Coriolis coupling model and a deformed axially symmetric, doubly even core [18]. Zell et al. [19] populated high-spin states in ^{75}Se via the ^{72}Ge(α,n)^{75}Se and

^{73}Ge($\alpha,2n$)^{75}Se reactions. States were observed up to ($\frac{21}{2}^+$, $\frac{19}{2}^+$) in the positive-parity band and up to $\frac{15}{2}^-$ for the negative-parity band. The yrast positive-parity states were interpreted to have a rotational bandhead at $I^\pi = \frac{9}{2}^+$. A comparison with the neighboring isotopes ^{74}Se and ^{76}Se revealed very similar band structures [19]. A lifetime measurement made for the 132 keV level by Agarwal et al. [20] also implied a large deformation for ^{75}Se.

The present work was undertaken to further investigate the high-spin properties of ^{75}Se. The reaction ^{59}Co(^{19}F,$2pn$)^{75}Se was used to populate states of higher angular momentum than had been done previously [19]. The level scheme has been extended and lifetime measurements were made. Comparisons with the neighboring isotones ^{77}Kr and ^{79}Sr suggest that the bandhead of the positive-parity rotational band is $I^\pi = \frac{5}{2}^+$. Band crossings similar to those known for ^{73}Se, ^{77}Kr, and ^{79}Sr were discovered and interpreted as the alignment of a $g_{9/2}$ proton pair. Transition quadrupole moments in the positive-parity band were extracted from the measured lifetimes and compared with predictions based on cranking calculations using a Woods-Saxon potential with pairing. The calculation results indicate a largely triaxial yrast structure, as contrasted with the nearly prolate shapes of the isotones ^{77}Kr and ^{79}Sr.

II. EXPERIMENTAL PROCEDURE

High-spin states in ^{75}Se were populated via the reaction ^{59}Co(^{19}F,$2pn$)^{75}Se. A thick ^{59}Co target was bombarded with a 55 MeV ^{19}F beam using the Florida State University Tandem accelerator. The $2pn$ evaporation channel was populated with about 10% of the yield.

Four 25% efficient high-purity Compton-suppressed Ge detectors were used to collect γ-γ coincidence data. The resolution of these detectors was about 2 keV at 1332 keV. One detector was placed at 25° with respect to the beam axis and three were placed at 90°, in such a way that backscatter was minimized. Data from the forward detector were used in the measurement of lifetimes and correlation ratios. Initial calibrations were made with a ^{152}Eu source, and during the experiment, on-line monitoring of the calibrations was made using the following lines: 112.1 keV (^{75}Se), 119.5 keV (^{75}Br), 286.4 keV (^{75}Se), 511.0 keV (e^+e^-), 562.93 keV (^{75}Br), 654.13 keV (^{75}Br), 728.4 keV (^{74}Se), 830.23 keV (^{75}Br), 1045.33 keV (^{75}Br), 1173.23 keV (^{60}Ni), and 1332.52 keV (^{60}Ni).

Over 4×10^8 coincidence events were recorded on magnetic tape and sorted into two two-dimensional arrays corresponding to 90°-90° angle pairs and 90°-25° angle pairs. When projections from the 90° spectra gated by lines in the 25° spectra could be made, these were added to the 90°-90° projections to improve overall statistics for the 90° spectra.

Wherever possible directional correlation of oriented nuclei (DCO) ratios were calculated to establish multipolarities. The DCO ratio is given by the intensity of a given line in the 25° spectrum gated on the 90° detec-

tor divided by the intensity of the same line in the 90° spectrum gated on the 25° detector. Gates on $E2$ transitions were used to measure DCO ratios. A DCO ratio of 1 is consistent with ΔI=2 and a fraction of this implies ΔI=1. Determination of DCO ratios for known transitions in ^{75}Br confirms this works even for the rather large forward angles of 25°.

III. CONSTRUCTION OF THE LEVEL SCHEME

A. The positive-parity band

A spectrum based on the addition of spectra projected from several transitions found in the positive-parity band of ^{75}Se is shown in Fig. 1. The ^{75}Se lines are identified and some transitions present due to gating on overlapping transitions from other nuclei have been labeled. The relative intensities, branching ratios, and DCO ratios for the positive-parity band are tabulated in Table I, along with branching ratios from other references for comparison, when available. The present branching ratio of 21% for the 132 keV transition was inferred from the ratio of intensities of the 132 and 112 keV lines in coincidence with the 801 keV transition.

Shown in Fig. 2 is the partial level scheme of ^{75}Se based on the present work. Spins and parities were assigned based on DCO ratio measurements. Although some ambiguities may be involved with DCO ratios, the matching of pairs of ΔI=1 transitions with single possi-
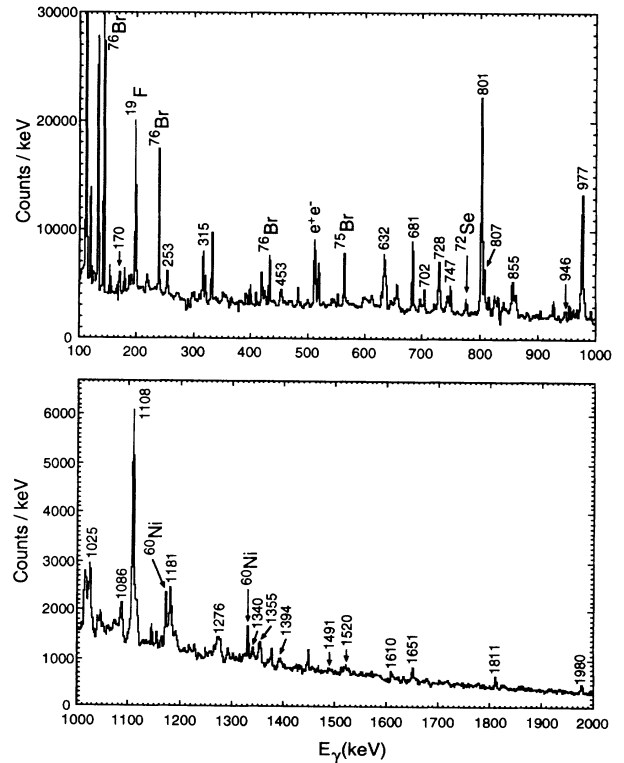

FIG. 1. Sum coincidence spectrum from the positive-parity band based on the addition of 90° spectra gated on the 112, 801, 977, 1108, 1181, 1276, 681, and 807 keV lines.

TABLE I.   Energies, intensities, branching ratios, and DCO ratios for the positive-parity band in ^{75}Se.

E_x (keV)	E_γ (keV)	I_γ	Branching ratio (%)	Branching[a] ratio (%)	Branching[b] ratio (%)	Branching[c] ratio (%)	R_{DCO}
112.1	112.1(1)	110(3)	100	100	100	100	0.72(3)
132.4	132.4(1)	30(2)	21(2)	100	55	30	0.81(7)
	20	–	79(2)		45	70	–
813.8	701.7(3)	9(3)	25(6)		27		1.22(20)
	681.1(2)	27(2)	75(6)		73		0.47(18)
933.5	801.1(1)	100	96(1)				0.99(13)
	119.4(2)	4(1)	4(1)				0.61(25)
1740.4	926.6(1)	9(2)	36(9)				1.27(38)
	806.9(2)	16(5)	64(9)				0.36(8)
1910.3	976.8(3)	69(5)	94(3)				1.10(5)
	169.8(3)	4(2)	6(3)				0.37(13)
2765.2	1024.8(7)	15(4)	44(7)				0.98(13)
	855.2(1)	19(2)	56(7)				0.22(25)
3017.9	1107.6(2)	38(2)	95(2)				1.12(17)
	252.7(5)	2(1)	5(2)				0.37(19)
3745.5	980.3(4)	6(3)	29(12)				–
	727.9(1)	15(4)	71(12)				0.21(10)
4198.6	1180.7(2)	12(2)	86(6)				1.35(32)
	453.2(7)	2(1)	14(6)				0.56(22)
4831.1	1085.6(5)	6(2)	44(16)				0.93(54)
	631.6(4)	8(5)	56(16)				0.31(10)
5474.6	1276.0(8)	9(2)	100				0.68(35)
1628.2	814.4(5)	9(3)	64(12)				0.51(24)
	694.2(3)	5(2)	36(12)				
2595.6	967.4(3)	6(3)	75(13)				
	684.9(2)	2(1)	25(13)				

[a]Reference [22].
[b]Reference [19].
[c]Reference [18].

ble $E2$ transitions provides further evidence that $\Delta J{=}2$ is correct for these cases. In addition, since yrast sequences are the most heavily populated in heavy ion reactions, stretched transitions of $\Delta J{=}2$ are expected rather than $\Delta J{=}0$. Several transitions in the yrast band that were known previously [19] in the $(\alpha = \frac{1}{2},\ \pi{=}+)$ band have

been confirmed. [α is the signature exponent quantum number related to angular momentum through the relation: $I{=}\alpha\,(\mathrm{mod}\,2)$.] In addition, two new levels have been added, extending the level scheme to $\frac{29}{2}^+$. The $\alpha = -\frac{1}{2}$ band has been identified in this work, and extended to $\frac{27}{2}^+$. Zell et al. [19] had previously observed the 814 keV
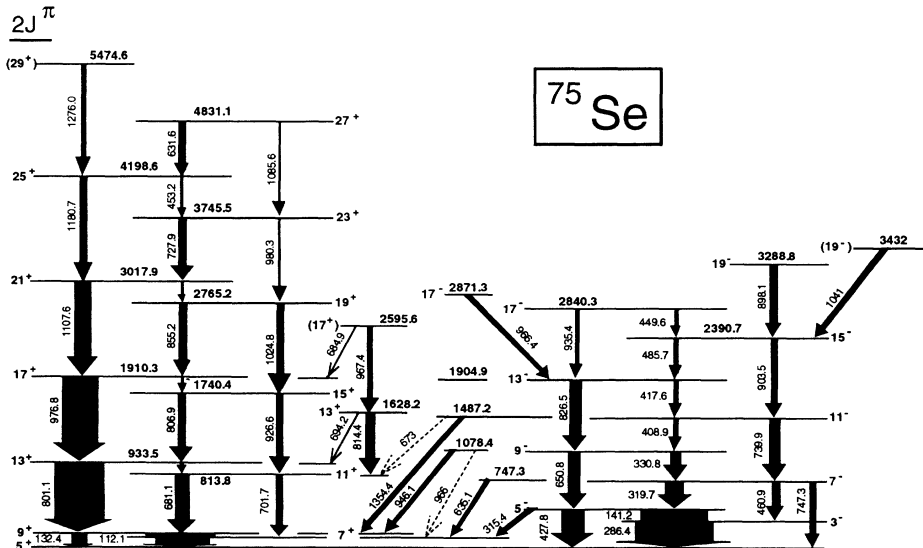

FIG. 2. Energy-level scheme of ^{75}Se deduced from the present work and previous studies.

level and had made a tentative spin-parity assignment of $\frac{11}{2}^+$. Two transitions also reported in Ref. [19] were an 856 keV line and an 810 keV line, and were placed according to γ-γ coincidence measurements. These are most likely the 855.2 and 806.9 keV lines observed in this experiment. Spin and parity assignments were not assigned previously [19], but have been identified here as the $\frac{19}{2}^+ \rightarrow \frac{17}{2}^+$ and $\frac{15}{2}^+ \rightarrow \frac{13}{2}^+$ transitions connecting states of opposite signature.

The new transitions placed in the level scheme are shown in the sum spectrum in Fig. 1 along with other lines to be discussed later. The 980.3 keV line, however, cannot be clearly distinguished from the strong 976.8 transition. It can be seen more clearly in Fig. 3, a γ spectrum in coincidence with the 976.8, 806.9, and 926.6 keV lines. The 980 keV line is also seen in each of these individual gates. The placement of the 980 keV transition above the 1025 keV line is supported by the smaller relative intensity of the 980 keV line and coincidence gates. In a spectrum of γ rays coincident with the 855 keV γ ray, the 977 and 980 keV lines can be distinguished. The 980 keV line is also coincident with the 1025 keV transition. In spectra coincident with the 1181 and 1108 keV transitions, the 977 keV line is symmetric with respect to the high and low energy ends and the 980 keV line is not observed. Seen also in Fig. 3 are other new members of the unfavored signature band. The identification of new $\Delta I=1$ transitions gives further confidence for the proposed placement of the $\Delta I=2$ lines.

The 814 keV line was first observed and placed in the level scheme in Ref. [19] based on the 814 keV transition appearing in coincidence with the 681 keV line. Coincidence measurements in this experiment confirm that coincidence relation and also show that the 702 and 814 keV lines are in coincidence with each other, which was a problem in Ref. [19], probably due to poorer statistics. An angular distribution measurement for the 814 keV transition was made previously [19]. However, an irregular excitation function was interpreted as indicating a doublet structure and no spin or parity was assigned. The angular distribution coefficients obtained were, nevertheless, consistent with a spin assignment of $\frac{13}{2}^+$. In
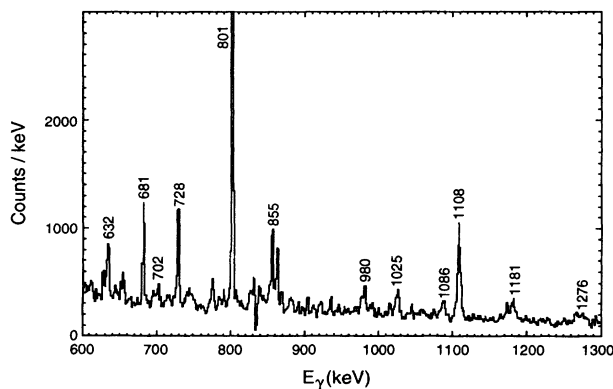
the present experiment, the DCO ratio has been measured for the 814 keV transition and is also consistent with a $\Delta I=1$ transition, and so we have assigned a spin-parity of $\frac{13}{2}^+$ for the 1628 keV level. No evidence confirming the earlier suspicion of a doublet structure of this line was found. The statistics were too poor to establish a DCO ratio for the 694 keV transition deexciting the same level. The DCO ratio for the 967 keV line was consistent with a spin-parity of $\frac{17}{2}^+$ for the 2596 keV level, but due to the large uncertainty in this measurement, the assignment has been left tentative, and again, due to poor statistics, no DCO ratio could be found for the 685 keV transition from this level.

Several transitions in Fig. 1 provide good candidates for further extending the positive-parity band. The 1340, 1394, and 1491 keV lines show up very nicely in gates based on lower-lying transitions such as the 801 keV line and clearly belong in ^{75}Se. However, gates based on higher-lying transitions had too few statistics to convincingly place them in the level scheme. The 1520 keV line, although it shows up in the sum spectrum, was not quite clear in any single gate. The narrower lines at 1811 and 1980 keV also are clearly in ^{75}Se based on low-lying gates, but it cannot be firmly established into which levels they are feeding.

B. The negative-parity band

A sum spectrum for the negative-parity band is shown in Fig. 4; the relative intensities, branching ratios, and

FIG. 3. Sum coincidence spectrum from the positive-parity band based on the addition of 90° spectra gated on the 977, 807, and 927 keV lines.
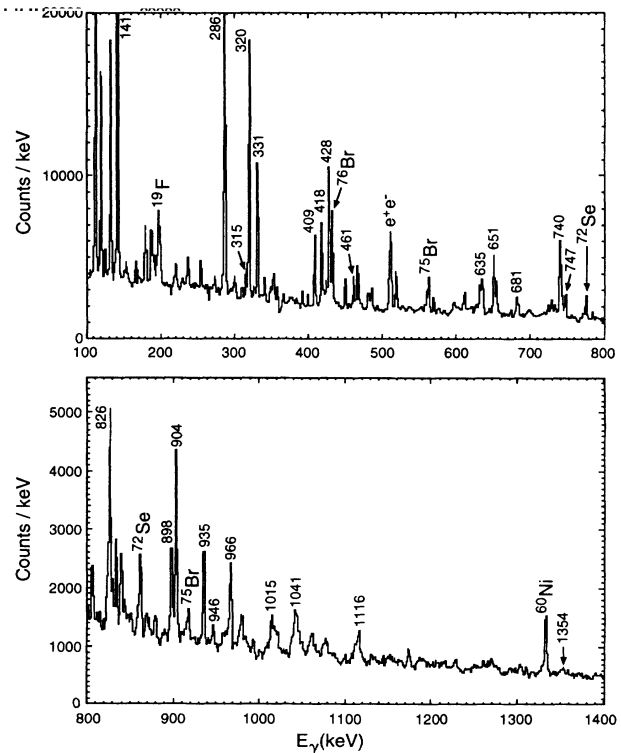

FIG. 4. Sum coincidence spectrum from the negative-parity band based on the addition of 90° spectra gated on the 286, 461, 740, 904, 651, 826, 320, 331, 409, and 428 keV lines.

DCO ratios are tabulated in Table II. The level scheme for the negative-parity band of ^{75}Se was previously [19] established to $\frac{15}{2}^-$. Coincidence measurements and DCO ratios measured here confirm the earlier level scheme and add six new transitions.

Two levels have been assigned a spin-parity of $\frac{19}{2}^-$; the 898.1 and 1041 keV transitions both feed the $\frac{15}{2}^-$ level. The 1041 keV transition might be thought to feed into the $\frac{19}{2}^-$ level. However, gates based on the 898 and 904 keV transitions show no 1041 keV line. It is also clear that the 1041 keV line is coincident with the 904 keV transition. Likewise, there is no evidence for a 898 keV line in the 1041 keV gate.

Spin-parities of $\frac{17}{2}^-$ have been assigned to two new levels. The 966 keV line is not seen in spectra coincident with the 935 keV transition. It is also observed in other coincidence spectra that neither the 966 nor 935 keV lines are in coincidence with the new 450 or 486 keV lines.

In the level scheme shown in Fig. 2, the transitions from yrast levels are drawn in the main cascade sequence. The 898 and 935 keV transitions fit the yrast prescription and the 2840 keV level also continues the $\Delta I=1$ decay sequence.

C. Parity changing transitions

Some parity changing transitions were known previously [16–22] and some new ones were added in this work. The 315 and 635 keV transitions observed earlier [18, 19, 21, 22] are also shown in the present level scheme. The spectrum coincident with the 826 keV transition shown in Fig. 6(a) has a 946 keV line also seen in the sum spectrum of Fig. 1, where the contribution here is from the 112 keV gate. This line has been identified as the $\frac{9}{2}^- \rightarrow \frac{9}{2}^+$ transition. Also the $\frac{11}{2}^- \rightarrow \frac{9}{2}^+$ 1354 keV transition can be clearly seen in Fig. 5(b) in coincidence with the 904 keV line, and is also seen in the sum spectrum shown in Fig. 1. The $\frac{11}{2}^- \rightarrow \frac{11}{2}^+$ and $\frac{9}{2}^- \rightarrow \frac{7}{2}^+$ transitions could only be tentatively placed due to poor statistics in the former case and because of overlapping with the two other 966 keV lines in the latter. There is some suggestive evidence that this 966 keV line has been observed from intensity relations. A projected spectrum in coincidence with the 702 keV line has both 814 and 967 keV lines. After double efficiency corrections, the ratio of the intensity of the 967 keV line to the 814 keV line is 0.33. In a similar analysis with a projected spec-

TABLE II. Energies, intensities, branching ratios, and DCO ratios for the negative-parity band in ^{75}Se.

E_x (keV)	E_γ (keV)	I_γ	Branching ratio (%)	Branching[a] ratio (%)	Branching[b] ratio (%)	Branching[c] ratio (%)	R_{DCO}
286.4(1)	286.4	–	100	100	100	100	0.79(2)
427.8(2)	427.6	44(4)	24(3)	38.9(14)	30.0	24.8	0.92(6)
	141.2(2)	132(2)	71(8)	53.6(19)	65.0	70.2	0.50(4)
	315.4(1)	10(3)	5(2)	7.5(3)	5.0	5.0	0.61(15)
747.3	460.9(3)	13(1)	22(2)	23.5(9)	26.9	17.6	1.02(9)
	319.7(1)	34(3)	59(7)	66.3(22)	73.1	60.3	0.35(2)
	635.1(2)	8(3)	14(5)	8.7(3)		–	0.65(5)
	747.3(3)	3(1)	5(2)	9.1(3)		22.1	–
1078.4	650.8(1)	20(1)	49(6)			62.9	0.97(7)
	330.8(2)	14(5)	34(13)			37.1	0.46(5)
	946.1(2)	7(1)	17(3)			–	–
	966	–	–			–	–
1487.2	739.9(2)	19(2)	59(9)			65.2	0.97(16)
	408.9(1)	8(2)	25(7)			34.8	0.40(6)
	673	–	–			–	–
	1354.4(4)	5(2)	16(7)			–	–
1904.9	826.5(1)	19(2)	68(8)			75.6	0.97(14)
	417.6(1)	9(3)	32(8)			24.4	0.37(11)
2390.7	903.5(1)	12(2)	71(5)			100	0.93(17)
	485.7(7)	5(1)	29(5)			–	0.52(22)
2840.3	935.4(2)	7(1)	70(8)				0.82(12)
	449.6(3)	3(1)	30(8)				0.59(14)
3288.8	898.1(2)	11(1)	100				0.98(15)
2871.3	966.4(1)	7(1)	100				1.09(27)
3431.2	1041	7(1)	100				0.78(20)

[a]Reference [22].
[b]Reference [18].
[c]Reference [19].

trum in coincidence with the 112 keV line, this ratio is 0.89. Of course, this cannot be considered conclusive evidence and also neglects the angular distribution of the 112 keV transition. Therefore the tentative assignment of the $\frac{9}{2}^{-} \to \frac{7}{2}^{+}$ transition stands.

IV. LIFETIME MEASUREMENTS

Mean lifetimes of high-spin states in ^{75}Se were measured for the first time using the Doppler-shift attenuation method (DSAM). Spectra from the forward detector gated by any other detector were used to analyze line shapes.

The ^{59}Co target foil was thick enough to stop all recoiling ^{75}Se nuclei and a fitting program [23] simulated the decay of the nucleus as it traversed the stopping medium. Electronic stopping powers were interpolated from Northcliffe and Schilling [24] and were scaled by a few percent to experimental [25] α stopping powers in ^{59}Co at the same velocity. Bohr's ansatz [26, 27] was used to calculate nuclear stopping powers and Blaugrund's approximation [28] was used to treat angular straggling at low recoil velocities. The recoil speeds following evaporation were assumed to follow a Gaussian distribution. The production of ^{75}Se, as the ^{19}F beam was decelerated in the target, was also simulated by the fitting code using production cross sections obtained from the statistical model code PACE [29].

Line shapes were used from spectra gated on transitions below the level of interest and the known transitions feeding into the state of interest were included in the simulation code to produce delayed feeding patterns. Side feeding was also taken into account assuming a side feeding lifetime of 0.05 and 0.10 ps for the $\frac{29}{2}^{+}$ and $\frac{27}{2}^{+}$ states, respectively. This side feeding lifetime was assumed to increase by 0.03 ps for each $\Delta I = 2$ transition down the respective cascades. The fast transitions observed here would not be consistent with slower side feeding times.

Some representative measured and simulated line shapes from this experiment are shown in Fig. 5. The results of the line-shape analysis are tabulated in Table

III, along with the reduced electric and magnetic transition strengths for all the transitions which could be analyzed. Dipole-quadrupole mixing ratios could not be measured for any of the $\Delta I = 1$ transitions for which lifetimes were measured. The calculations for $M1$ strengths were made assuming $\delta \approx 0.10(10)$ since they are not sensitive to the value of δ as long as it is small. A value of 0.10 for δ is consistent with the mixing ratio calculated from the angular distribution measurement results of Ref. [19] for the 681 keV transition. Sahota et al. [22] reported $|\ \delta\ | = 0.25(4)$ for the 112 keV transition. Small values for $|\ \delta\ |$ have also been reported for $E2/M1$ transitions in rotational bands for neighboring isotopes of ^{75}Se. In negative-parity band of ^{73}Se, Seiffert et al. [30] found a range of values $|\ \delta\ | = 0.16$ to 0.38. In the positive-parity band in ^{73}Se, Kaplan et al. [7] had measured three values for $|\ \delta\ |$ ranging from 0.08(5) to 0.43(31). The largest value for $|\ \delta\ |$ here, would change the $B(M1)$ value only by 10 %, and this is within the range of our error bars. In another isotope, ^{77}Se, Zell et al. [8] reported three values for $|\ \delta\ |$ in a negative-parity rotational band ranging from 0.094 to 0.188. In light of these measurements, it seems reasonable to assume small values for $|\ \delta\ |$ for the sake of demonstrating the overall behavior of the $B(M1)$ strengths.

Line shapes in the negative-parity band could not be easily fitted. No observable line shift was seen for any transition except for the highest spins in both signatures. The effective lifetimes measured for these levels were 0.62 and 0.69 ps for the 935 and 966 keV transitions, respectively. These fits were generally poor, however. A more believable effective lifetime of 0.89 ps was obtained for the 898 keV transition and no fit could be made for the 1041 keV line due to poor statistics.

V. DISCUSSION

One of the most interesting features of nuclei from the Ge-Zr region is the richness of various structural effects that occur at high angular momenta. Many of these ef-
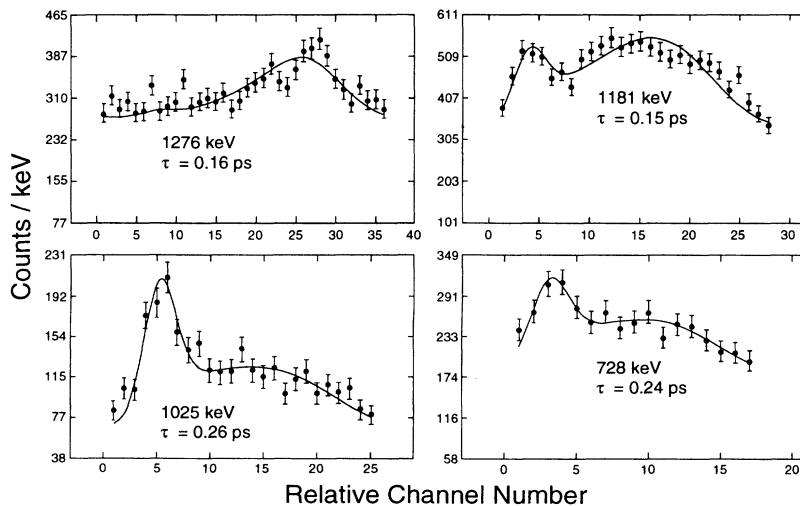

FIG. 5. Doppler-shifted line shapes observed at 25°. The smooth curves are theoretical line shapes fitted to the data, as discussed in the text. The data are taken from coincidence data.

TABLE III. Lifetimes and reduced transition strengths.

E_x (keV)	J^π	E_γ (keV)	τ_{PS}	$B(E2)$ (W.u.)	$B(M1)$ (μ_N^2)[b]
112.1	$\frac{7}{2}^+$	112.1	0.69^a_{ns}	242^{+100}_{-244}	$0.05^{+0.01}_{-0.01}$
132.4	$\frac{9}{2}^+$	132.4	$5.3(6)^a_{ns}$		
		20			$1.06^{+0.11}_{-0.14}$[c]
813.8	$\frac{11}{2}^+$	701.7	$-$		$-$
		681.1	$-$	$-$	
933.5	13.2^+	801.1	$-$	$-$	
		119.4	$-$	$-$	
1740.4	$\frac{15}{2}^+$	926.6	0.36(7)	64^{+15}_{-10}	
		806.9			$0.19^{+0.03}_{-0.05}$
1910.3	$\frac{17}{2}^+$	976.8	0.43(8)	110^{+29}_{-19}	
		169.8			$1.61^{+0.25}_{-0.37}$
2765.2	$\frac{19}{2}^+$	1024.8	0.26(5)	65^{+16}_{-11}	
		855.2			$0.19^{+0.03}_{-0.05}$
3017.9	$\frac{21}{2}^+$	1107.6	0.33(8)	75^{+24}_{-15}	
		252.7			$0.53^{+0.10}_{-0.17}$
3745.5	$\frac{23}{2}^+$	980.3	0.24(5)	58^{+11}_{-8}	
		727.9			$0.44^{+0.08}_{-0.12}$
4198.6	$\frac{25}{2}^+$	1180.7	0.15(3)	109^{+27}_{-18}	
		453.2			$0.57^{+0.09}_{-0.14}$
4831.1	$\frac{27}{2}^+$	1085.6	$0.46(9)^d$	>28	
		631.6			>0.27
5474.6	$\frac{29}{2}^+$	1276.0	$0.16(3)^d$	>80	
2840.3	$\frac{17}{2}^-$	935.4	$0.62(29)^d$	>68	
2871.3	$\frac{17}{2}^-$	966.4	$0.69(31)^d$	>75	
3288.8	$\frac{19}{2}^-$	898.1	$0.89(27)^d$	>84	

[a]Reference [20].
[b]Used $\delta = -0.25(4)$.
[c]Used $\delta=0.00$.
[d]Effective lifetime.

fects have a straightforward interpretation in terms of the interplay between deformation, pairing, and the Coriolis force.

In the $A \sim 80$ region both protons and neutrons lie in the same $g_{9/2}$ high-j subshell. Consequently, proton and neutron band crossings are expected at similar frequencies. For γ-soft systems such configuration changes induce strong shape variations caused by aligned quasiparticles which polarize the core.

Classical examples of high-spin shape coexistence in the $A \sim 80$ mass region can be found in nuclei around $N = 42$. According to the experimental systematics and the deformed shell model theory, the Kr, Sr, and Zr nuclei with the neutron number $N = 42$–44 lie on the border of the deformed $A \sim 80$ island centered around ^{76}Sr. These transitional nuclei are deformation soft, and, therefore, they are very sensitive to all the effects which are associated with shape variations.

The valence quasiparticle orbitals belonging to high-j abnormal parity subshells exert strong γ-driving forces on the core. As the Fermi surface rises through a high-j shell, the γ deformation to which the orbitals drive changes smoothly from γ=60° (oblate noncollective), through γ=0° (prolate collective) and γ=−60° (oblate

collective), finally to γ=−120° (prolate noncollective) [31].

In odd-A nuclei with $N = 43$–45 very strong polarization effects coming from aligned quasiparticle excitations have been observed. They manifest themselves by shape changes induced by the quasiparticle alignment and by variations in the signature splitting and the $B(M1)$ strength with angular momentum, seen, e.g., in ^{79}Kr (Ref. [32]), ^{79}Kr (Ref. [33]), ^{81}Kr (Ref. [34]), ^{79}Rb (Ref. [35]) , ^{81}Rb (Ref. [36]), ^{81}Sr (Ref. [23]), ^{83}Y (Ref. [37]), and ^{83}Zr (Ref. [38]).

A spectacular example of configuration-dependent quasiparticle alignment related to γ softness has recently been established in ^{79}Rb [35]. The favored ($\alpha = \frac{1}{2}$) $g_{9/2}$ band exhibits a smooth neutron alignment, while a sharper band crossing is seen in the unfavored ($\alpha = -\frac{1}{2}$) $g_{9/2}$ sequence, which results in a dramatic variation of the signature splitting. This behavior can be explained in terms of different deformations for the two signatures of the $g_{9/2}$ band. According to the calculations [39], the excitation energy of the odd $g_{9/2}$ proton in ^{79}Rb favors near-prolate shapes ($\gamma\sim0°$) for the ($\alpha = \frac{1}{2}$) band. On the other hand, the unfavored band prefers a near-oblate ($\gamma\sim-50°$) shape above the neutron crossing frequency.

A. Systematics

The level scheme of ^{75}Se is quite similar to those of the neighboring isotones ^{77}Kr and ^{79}Sr. Figure 6 shows a comparison between the $g_{9/2}$ bands of all three isotones. (For the systematic *isotopic* comparison, see Refs. [8, 9].) The $\frac{13}{2}^+ \rightarrow \frac{9}{2}^+$ transition energy is seen to decrease from ^{75}Se to ^{79}Sr, suggesting increasing deformation as the proton number increases towards midshell. This is to be expected from general systematics [40–42], One feature that stands out is a decrease in the signature splitting with increasing proton number. This should be reflected in the size of the $M1$ strength staggering for transitions between signatures [43, 44]. Indeed, as demonstrated by Hagemann and Hamamoto [45], there is a unique γ-*dependent* relationship between the normalized signature splitting of the Routhians,

$$\widetilde{\Delta e'} = \frac{4\Delta e' \hbar\omega}{(\hbar\omega)^2 + (\Delta e')^2},\tag{1}$$

and the normalized signature splitting of $M1$ rates,

$$\Delta\widetilde{B(M1)} = \frac{\Delta B(M1)}{B(M1)_{av}},\tag{2}$$

i.e.,

$$\widetilde{\Delta e'} \Longleftrightarrow \Delta\widetilde{B(M1)}.\tag{3}$$

In Eqs. (1)–(3) $\Delta B(M1) = B(M1;\alpha_f \rightarrow \alpha_u) - B(M1;\alpha_u \rightarrow \alpha_f)$, $B(M1)_{av} = \frac{1}{2}[B(M1;\alpha_f \rightarrow$
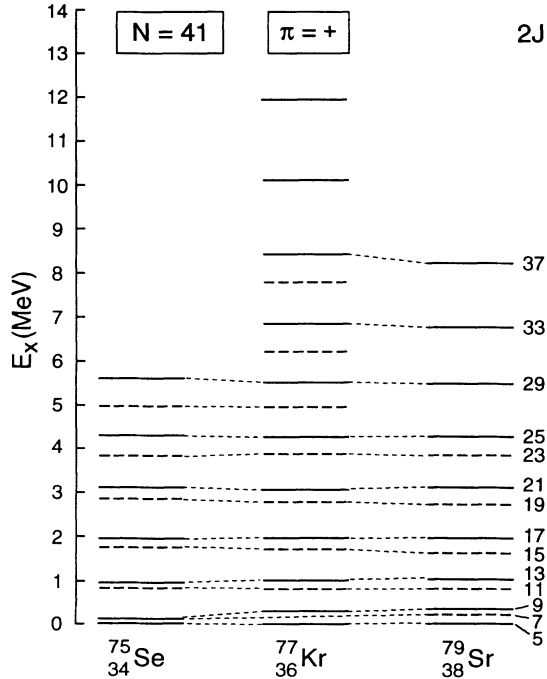
$\alpha_u) + B(M1;\alpha_u \rightarrow \alpha_f)]$, ω is the rotational frequency, and $\Delta e'$ is the signature splitting energy, i.e., the difference in energy between the Routhians of the favored and unfavored sequences

$$\Delta e' \equiv e'(\alpha_u) - e'(\alpha_f).\tag{4}$$

In the limit of axial symmetry, relation (3) becomes an identity. For triaxial shapes, however, there is a very strong dependence of both sides of Eq. (3) on the position of the Fermi level [45].

Large $B(M1)$ staggering was reported for, e.g., ^{77}Kr (Refs. [46, 47]), ^{79}Sr (Ref. [48]), and ^{79}Kr (Refs. [32, 33]) and was interpreted in the framework of the cranking model [49, 50]. The $B(M1)$ rates for ^{75}Se are plotted versus spin in Fig. 7. The two nonshaded triangles in the plot are inferred $B(M1)$ strengths. Since lifetime measurements could not be obtained for these levels, $B(E2)$ strengths for the 801 and 702 keV transitions were assumed to have values which averaged near those which we could find. Lifetimes could then be calculated for the $\frac{13}{2}^+$ and $\frac{11}{2}^+$ levels; and $B(M1)$ strengths were calculated assuming these inferred lifetimes. The staggering is quite large below the band crossing, and decreases for the smaller signature splitting above the band crossing. Below the band crossings, the staggering appears larger than that for ^{77}Kr (Ref. [47]) and ^{79}Sr (Ref. [48]), as expected from the larger signature splitting.

B. Cranked shell model analysis

Alignments and structural changes due to rotation are more clearly seen by using the cranked shell model (CSM). Kinematical and dynamical moments of inertia, $\mathcal{J}^{(1)} \equiv I_x/\omega$ and $\mathcal{J}^{(2)} \equiv dI_x/d\omega$, for the positive-parity band of ^{75}Se are shown in Fig. 8 along with those of the neighboring isotones ^{77}Kr and ^{79}Sr. The behavior of

FIG. 6. Comparison of the positive-parity excitation energy levels for ^{75}Se, ^{77}Kr, and ^{79}Sr. The ^{77}Kr levels are from Ref. [47]. The ^{79}Sr levels are taken from Refs. [48] and [53].
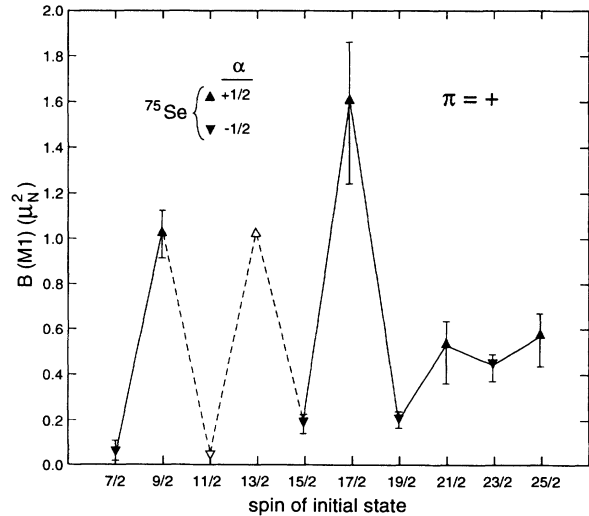

FIG. 7. $B(M1)$ strengths in ^{75}Se. The first two data points are from lifetime measurements in Ref. [20]. The two open arrows refer to inferred quantities, as discussed in the text.

these moments of inertia is seen to be quite similar. For rotational bands of ^{77}Kr and ^{79}Sr based on the $[422]\frac{5}{2}$ Nilsson state, we assumed $K = \frac{5}{2}$. For ^{75}Se, because of much larger signature splitting in the $g_{9/2}$ band and predicted triaxial shape, see Sec. V D, K is not a good quantum number. Consequently, in the CSM analysis the average value $K = \frac{3}{2}$, representative of the rota-
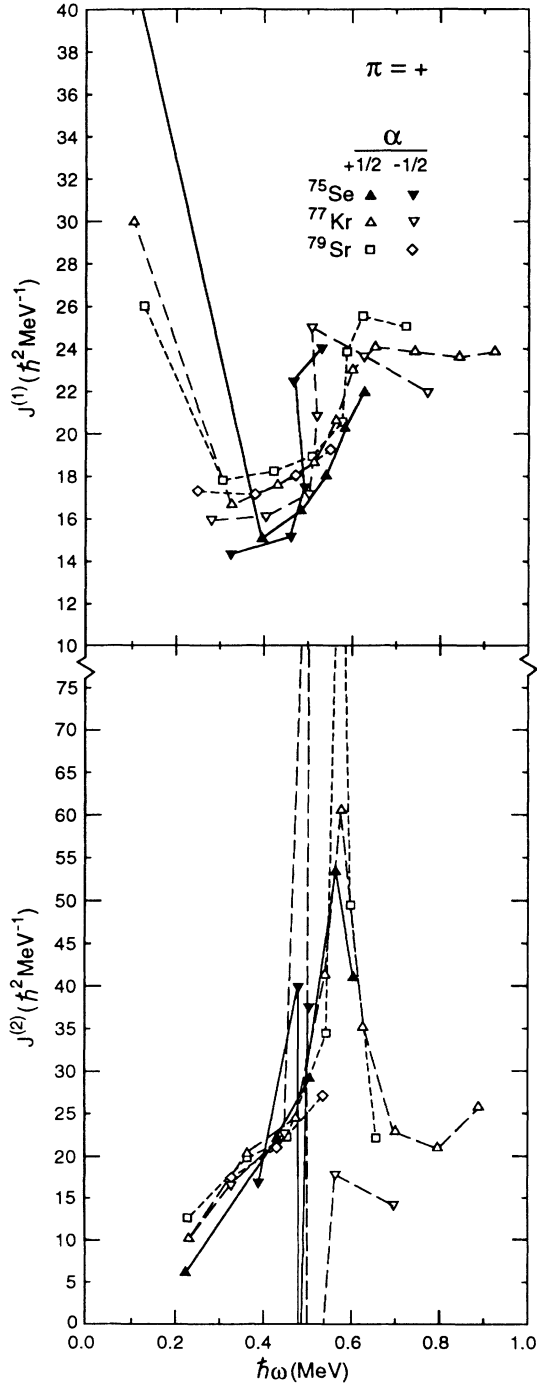
tional alignment limit, was employed. For both ^{75}Se and ^{77}Kr the alignment of the favored positive-parity band is rather gradual, while the unfavored positive-parity bands exhibit sharper alignment at a significantly lower rotational frequency. Indeed, the crossing frequency for the unfavored band in ^{75}Se is about $\hbar\omega_c=0.48$ MeV compared to $\hbar\omega_c\sim0.56$ MeV for the favored band. For ^{77}Kr the corresponding crossing frequencies are about 0.53 and 0.59 MeV, respectively. This signature dependence of the crossing frequency will be discussed in Sec. V D.

The unfavored $g_{9/2}$ band for ^{79}Sr is not known well enough, but it appears that the alignment may be more gradual. Another interesting feature is a trend for the favored $g_{9/2}$ bands to exhibit a sharper alignment with increasing proton number. This may imply that the band interaction becomes weaker in the favored signature as deformation increases.

Because of neutron blocking, the band crossing in all three isotones can be explained by the alignment of a pair of $g_{9/2}$ protons. This is the first time this quasiparticle alignment has been observed in ^{75}Se. The comparison of the moments of inertia for the isotones ^{75}Se, ^{77}Kr, and ^{79}Sr indicates, however, that the known level scheme
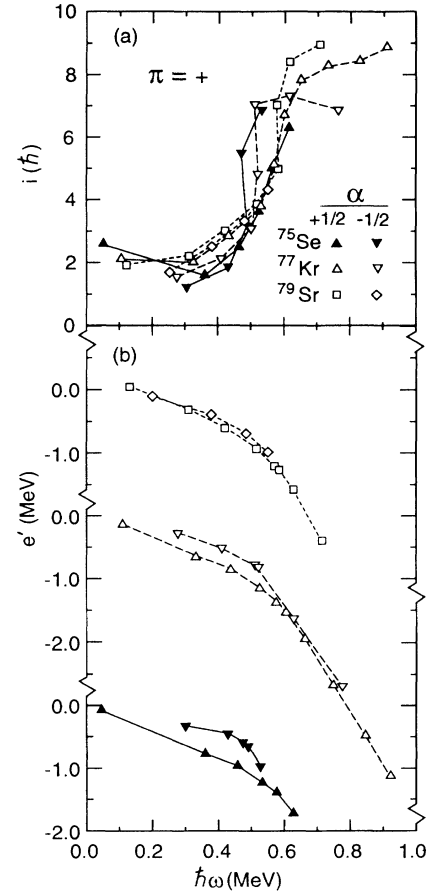

FIG. 8. Plots of the kinematical ($\mathcal{J}^{(1)}$) and dynamical ($\mathcal{J}^{(2)}$) moments of inertia for the lowest positive-parity bands in ^{75}Se, ^{77}Kr, and ^{79}Sr.

FIG. 9. (a) Aligned momenta i and (b) Routhians e' for the lowest positive-parity bands in ^{75}Se, ^{77}Kr, and ^{79}Sr. The reference parameters are $\mathcal{J}_0=10\hbar^2$/MeV and $\mathcal{J}_1=5\hbar^4$/MeV^3.

for ^{75}Se does not extend into the region above the band crossing.

The gain in angular momentum due to quasiparticle decoupling can be seen more directly by plotting the aligned angular momentum $i = I_x - I_{ref}$. The parameters describing the reference rotor were those used in Refs. [46] and [47] for ^{77}Kr, i.e., $\mathcal{J}_0 = 10\hbar^2$/MeV and $\mathcal{J}_1 = 5\hbar^4$/MeV^3. The alignments obtained for the three isotones discussed are shown in Fig. 9(a). The higher initial value of alignment for ^{75}Se leads to the very large $\mathcal{J}^{(1)}$ value in Fig. 8.

The signature splitting mentioned earlier can also be seen by plotting the total Routhians versus the rotational frequency as shown in Fig. 9(b). It is seen that the signature splitting increases as Z decreases. For ^{75}Se the signature splitting at a rotational frequency $\hbar\omega$=0.4 MeV, $\Delta e'$, is around 320 keV. This decreases to about 200 keV for ^{77}Kr and to 120 keV in ^{79}Sr. For both ^{75}Se and

^{77}Kr, $\Delta e'$ decreases at the band crossing, as discussed in Sec. V D.

Structural changes for the negative-parity band are illustrated in the $\mathcal{J}^{(1)}$ and $\mathcal{J}^{(2)}$ plots shown in Fig. 10. In all three cases, K was taken to be $\frac{3}{2}$. One feature clearly observed is that $\mathcal{J}^{(1)}$, at low spin, increases with Z. Both the $\mathcal{J}^{(1)}$ and $\mathcal{J}^{(2)}$ plots demonstrate a tendency for sharper alignment with decreasing Z. The last point for both signatures in ^{75}Se was calculated using the levels drawn in the main cascade sequence in the level scheme of Fig. 2. These points indicate the onset of a band crossing at $\hbar\omega\sim$0.42 MeV. For ^{77}Kr and ^{79}Sr the band crossing occurs at a higher frequency, around 0.55 and 0.52 MeV, respectively. One interesting comparison that can be made from these figures is that the alignment for the $\alpha = -\frac{1}{2}$ signature band of ^{75}Se appears to be sharper than that of the opposite signature. This is in contrast to the behavior of the negative-parity band in ^{77}Kr.

Aligned angular momenta for the negative-parity bands are shown in Fig. 13(a). Although ^{75}Se starts off with a smaller alignment than the neighboring isotones, the alignment is quite rapid, even below the onset of the band crossing. The total Routhians for the negative-parity bands of the three isotones of interest are shown in Fig. 11(b). As expected, they show much less signature splitting than in the positive-parity bands and the favored band has signature $\alpha = +\frac{1}{2}$.
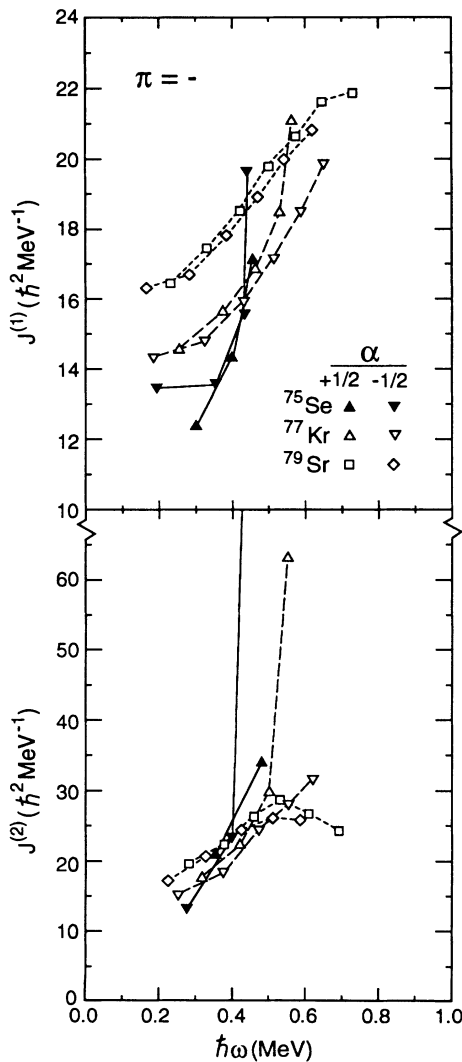

FIG. 10. Plots of the kinematical ($\mathcal{J}^{(1)}$) and dynamical ($\mathcal{J}^{(2)}$) moments of inertia for the lowest negative-parity bands in ^{75}Se, ^{77}Kr, and ^{79}Sr.
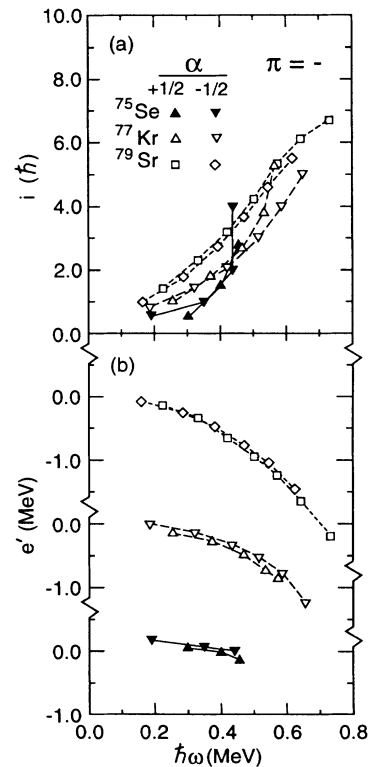
FIG. 11. (a) Aligned angular momentum i and (b) Routhians e' for the lowest negative-parity bands in ^{75}Se, ^{77}Kr, and ^{79}Sr. The reference parameters are $\mathcal{J}_0$=10$\hbar^2$/MeV and $\mathcal{J}_1$ =5$\hbar^4$/MeV^3.

C. Transition strengths and quadrupole moments

The $B(E2)$ values for ^{75}Se found in this experiment have been tabulated in Table III. Transition quadrupole moments were also calculated from the simple rotational model and can be seen in Table IV along with those of ^{77}Kr and ^{79}Sr. The first value of Q_t shown for ^{75}Se in Table IV is simply the ground-state quadrupole moment for ^{75}Se found by Aamodt and Fletcher [13]. This seems somewhat small. The next value for Q_t in ^{75}Se is calculated from the lifetime for the 132 keV level measured by Agarwal *et al.* [20]. The Q_t values calculated for the 132 and 977 keV transitions are consistent with each other and with a large deformation. This agrees with a recent investigation of the low-spin states in ^{75}Se (Ref. [22]), where a $\beta_2 \gtrsim 0.35$ was inferred. A more quantitative discussion of the deformations implied by the measured lifetimes will be given in Sec. V D. The quadrupole moments for the three isotones in Table IV reflect the large deformations of these nuclei. The quadrupole moments for low-spin favored-signature states in ^{75}Se are surprisingly large when compared to ^{77}Kr, although at higher spins, they decrease somewhat and drop below those for ^{77}Kr. Quadrupole moments in the unfavored signature in ^{75}Se show a trend for decreasing values, although the error bars do not permit a firm conclusion. Unfortunately, lifetimes for the lower unfavored signature spin states in ^{75}Se could not be measured and only one lifetime in the analogous band for ^{79}Sr is known. The Q_t values for ^{75}Se are plotted in Figs. 12 and 13 along with theoretically calculated moments to be discussed in Sec. V D.

D. Woods-Saxon calculations

Woods-Saxon-Bogolyubov cranking calculations were performed to investigate the high-spin properties of ^{75}Se, using the Woods-Saxon model discussed in Ref. [51]. A monopole pairing force was assumed and the cranking approximation was used to describe the rotation. The procedure is described in more detail in Refs. [23] and [52].

Figure 14 displays the calculated one-quasiparticle Woods-Saxon Routhians for $N = 41$ as functions of γ at constant values of $\beta_2 = 0.28$ and $\hbar\omega = 0.3$ MeV. For neutron number $N = 41$ the Fermi level penetrates into the upper half of the $g_{9/2}$ shell, which favors deformations with large negative γ values. Indeed, the lowest favored $g_{9/2}$ Routhian (solid curve) is lowest at $\gamma \sim -40°$. For the unfavored $g_{9/2}$ Routhian (dotted line) the deformation dependence is very weak and the corresponding rotational band is expected to follow the deformation of the core. On the other hand, the aligned $g_{9/2}$ protons are expected to drive the system towards positive values of γ [34, 40].

Examples of the calculated total Routhian surfaces (TRS) in the (β_2, γ) plane for the yrast configurations $A(\pi=+, \alpha = \frac{1}{2})$, $B(\pi=+, \alpha = -\frac{1}{2})$, and $F(\pi=-, \alpha = \frac{1}{2})$ are shown in Fig. 15. The grid points at each (β_2, γ) value were minimized with respect to the hexadecapole deformation parameter β_4. The rotational frequencies chosen, $\hbar\omega = 0.3$ and 0.6 MeV, correspond to the situation before and after the $g_{9/2}$ proton alignment. The TRS for configuration $E(\pi=-, \alpha = -\frac{1}{2})$ is qualitatively

TABLE IV. Transition quadrupole moment $|Q_t|$ comparisons ($\Delta J = 2$ transitions).

	$J_i^\pi \rightarrow J_f^\pi$	^{75}Se (e b)	^{77}Kr (e b)[a]	^{79}Sr (e b)[b]
$\alpha = +\frac{1}{2}$	$\frac{5}{2}^+$	$1.1(2)$[c]	2.0	
	$\frac{9}{2}^+ \rightarrow \frac{5}{2}^+$	$2.83^{+0.18}_{-0.15}$[d]	$2.01^{+0.24}_{-0.18}$	$3.21^{+0.30}_{-0.27}$
	$\frac{13}{2}^+ \rightarrow \frac{9}{2}^+$	—	$2.52^{+0.74}_{-0.39}$	$3.48^{+0.41}_{0.31}$
	$\frac{17}{2}^+ \rightarrow \frac{13}{2}^+$	$2.78^{+0.35}_{-0.25}$	$2.82^{+0.33}_{-0.24}$	$2.68^{+0.25}_{-0.15}$
	$\frac{21}{2}^+ \rightarrow \frac{17}{2}^+$	$2.18^{+0.32}_{-0.22}$	$2.82^{+0.37}_{-0.27}$	$1.78^{+0.24}_{-0.18}$
	$\frac{25}{2}^+ \rightarrow \frac{21}{2}^+$	$2.55^{+0.30}_{-0.22}$	$2.64^{+0.29}_{-0.18}$	≥ 2.0
	$\frac{29}{2}^+ \rightarrow \frac{25}{2}^+$	≥ 2.15	$1.62^{+0.21}_{-0.15}$	
	$\frac{33}{2}^+ \rightarrow \frac{29}{2}^+$		$2.17^{+0.34}_{-0.23}$	
	$\frac{37}{2}^+ \rightarrow \frac{33}{2}^+$		≥ 1.8	
	$\frac{41}{2}^+ \rightarrow \frac{37}{2}^+$			
	$\frac{45}{2}^+ \rightarrow \frac{41}{2}^+$			
$\alpha = -\frac{1}{2}$				
	$\frac{11}{2}^+ \rightarrow \frac{7}{2}^+$	—	$2.88^{+0.34}_{-0.25}$	$3.31^{+0.29}_{-0.26}$
	$\frac{15}{2}^+ \rightarrow \frac{11}{2}^+$	$2.20^{+0.25}_{-0.19}$	$2.14^{+0.26}_{-0.19}$	≥ 2.4
	$\frac{19}{2}^+ \rightarrow \frac{15}{2}^+$	$2.10^{+0.24}_{-0.18}$	$1.49^{+0.19}_{-0.13}$	
	$\frac{23}{2}^+ \rightarrow \frac{19}{2}^+$	$1.89^{+0.18}_{-0.14}$	$1.83^{+0.22}_{-0.16}$	
	$\frac{27}{2}^+ \rightarrow \frac{23}{2}^+$	≥ 1.53	$2.44^{+0.30}_{-0.22}$	
	$\frac{31}{2}^+ \rightarrow \frac{27}{2}^+$		≥ 2.1	
	$\frac{35}{2}^+ \rightarrow \frac{31}{2}^+$			

[a]Reference [47].
[b]Reference [48].
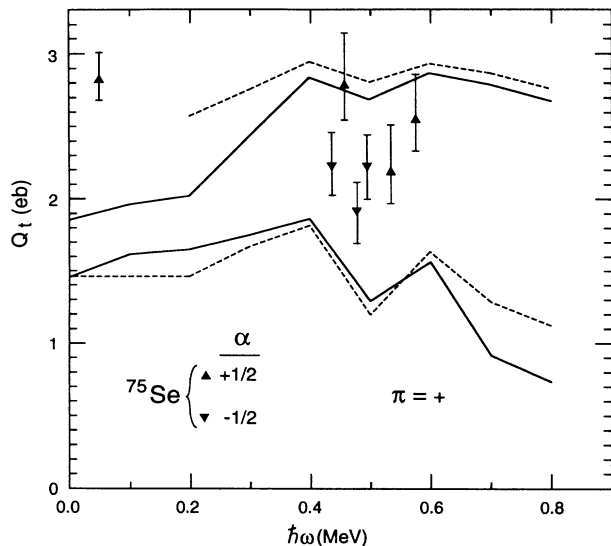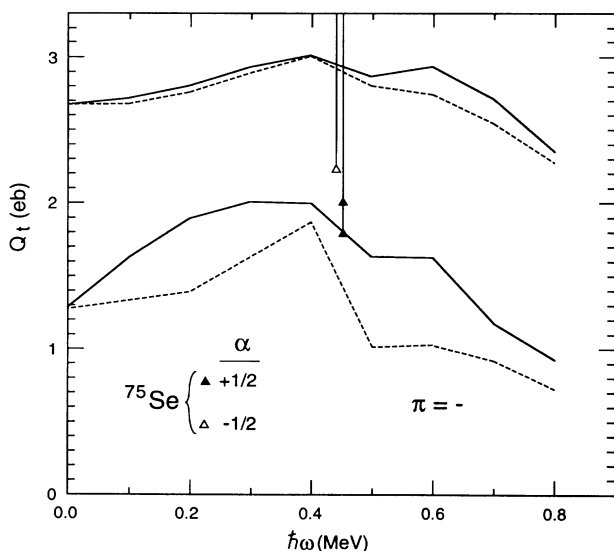[c]Reference [13].
[d]Reference [20].

FIG. 12. Transition quadrupole moments for the $\Delta I{=}2$ transitions in the positive-parity band, inferred from the measured lifetimes. The lines represent theoretical values as discussed in the text. The solid line corresponds to the $A(\alpha = +\frac{1}{2})$ configuration and the dashed line corresponds to $B(\alpha = -\frac{1}{2})$.

similar to that of F, and, therefore, is not shown in Fig. 15.

As expected, the lowest $g_{9/2}$ neutron excitation drives ^{75}Se towards negative values of γ. At the rotational frequency $\hbar\omega{=}0.3$ MeV the favored band A has a clearly

defined minimum at $\beta_2 = 0.26$ and $\gamma{=}{-}33°$. For the unfavored band B the corresponding TRS is very γ soft and there are two minima very close in energy; i.e., the near-oblate minimum with $\beta_2 = 0.23$ and $\gamma ={-}54°$, and the triaxial minimum with $\beta_2 = 0.29$ and $\gamma ={-}23°$. One can thus conclude that at frequencies below the first band crossing the positive-parity bands can be associated with strongly triaxial shapes with $\gamma{<}0$.

The situation changes markedly after the $g_{9/2}$ proton alignment, which takes place at $\hbar\omega{\sim}0.52$ MeV and $\hbar\omega{\sim}0.4$ MeV for the $\gamma{\sim}{-}30°$ and $\gamma{\sim}30°$ configurations, respectively.

At $\hbar\omega{=}0.6$ MeV the absolute minimum of the three-quasiparticle band $\nu g_{9/2}(A)\pi(g_{9/2})^2$ has $\beta_2 = 0.30$ and $\gamma ={-}27°$, i.e., it is fairly close to the minimum of the one-quasiparticle band A. The secondary minimum at $\gamma{\sim}27°$ is about 0.2 MeV higher in energy. According to the calculations this minimum becomes yrast at $\hbar\omega{>}0.63$ MeV, i.e., after decoupling of the second $g_{9/2}$ neutron pair (BC crossing). For the three-quasiparticle band $\nu g_{9/2}(B)\pi(g_{9/2})^2$ the scenario is slightly different. Here, the proton alignment has a more dramatic effect due to the insensitivity of excitation B to γ. It is seen from Fig. 15 that at $\hbar\omega{=}0.6$ MeV the absolute minimum of configuration B can be associated with a *positive* value of $\gamma{\sim}28°$. The secondary minimum with *negative* $\gamma{\sim}{-}26°$ lies ~ 0.3 MeV higher in energy. The actual shape transition is predicted at $\hbar\omega{\sim}0.4$ MeV, i.e., just after the proton alignment at the $\gamma{>}0$ shape.

The predicted behavior of the $\pi{=}{+}$ bands in ^{75}Se is consistent with the observed alignment pattern shown in Figs. 8 and 9, namely, with the following:

(i) The large signature splitting between the $g_{9/2}$ bands before the proton crossing is characteristic of triaxial shape with a large negative value of γ, cf. Fig. 14. (ii)

FIG. 13. Transition quadrupole moments for the $\Delta I{=}2$ transitions in the negative-parity band, inferred from the measured lifetimes. The lines represent theoretical values as discussed in the text. The solid line corresponds to the $F(\alpha = +\frac{1}{2})$ configuration and the dashed line corresponds to $E(\alpha = -\frac{1}{2})$.
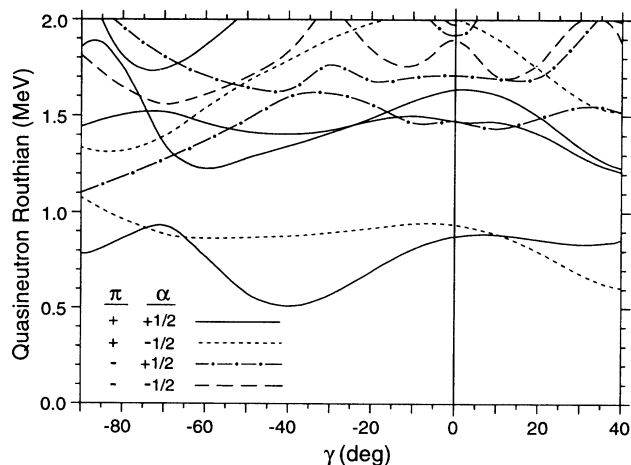

FIG. 14. One-quasiparticle Routhians for neutrons calculated at a frequency (0.3 MeV) slightly below the first proton band crossing. They are shown as a function of the triaxiality parameter γ for constant values of $\beta_2{=}0.28$ and $\beta_4{=}0$. The following line convention is used: $(\pi{=}{+},\ \alpha = \frac{1}{2})$, solid; $(\pi{=}{+},\ \alpha = -\frac{1}{2})$, dotted; $(\pi{=}{-},\ \alpha = \frac{1}{2})$, dash-dotted; $(\pi{=}{-},\ \alpha = -\frac{1}{2})$, dashed.

The very early sharp crossing in the unfavored $g_{9/2}$ band at $\hbar\omega\sim0.48$ MeV can be explained in terms of a shape change from the $\gamma<0°$ configuration to the $\gamma>0°$ configuration induced by the decoupling of $g_{9/2}$ protons. The gradual alignment in the favored $g_{9/2}$ band at $\hbar\omega\sim0.55$ MeV does not involve any dramatic shape change; i.e., it can be associated with the large-interaction band crossing at the $\gamma\sim-30°$ configuration. The actual shape transition within the favored band is predicted to occur later, at $\hbar\omega>0.63$ MeV, i.e., very close to the point where the present experimental data end. (iii) According to the calculations, at high rotational frequencies, $\hbar\omega>0.65$ MeV, both $\pi=+$ bands are built upon the $\gamma\sim30°$ shape. One should, therefore, expect a crossing between the two $g_{9/2}$ signatures, i.e., a *signature inversion*, see Fig. 14. (iv) Both the decrease in the signature splitting between the $g_{9/2}$ Routhians and the increase in the proton crossing frequency with proton number reflect the shape transition from the strongly triaxial shapes in ^{75}Se ($\beta_2\sim0.28$, $\gamma\sim-30°$) through slightly triaxial shapes in ^{77}Kr ($\beta_2\sim0.34$, $\gamma\sim-8°$, Ref. [46]) towards well-deformed near-axial shapes ($\gamma\sim-5°$) in ^{79}Sr ($\beta_2\sim0.37$, $\gamma\sim0°$, Refs. [48, 53]). (For the deformation dependence of the $g_{9/2}$ crossing frequency, see [54].)

The $g_{9/2}$ bands in ^{73}Se [7] look fairly similar to the $g_{9/2}$ bands in ^{75}Se found in this study; i.e., after the proton alignment the strongly decoupled structure changes to a more coupled band with reduced signature splitting. Also there is about a 100 keV shift in the proton crossing frequency for different signature partners. In fact, our TRS calculations predict rather similar alignment patterns in ^{73}Se and ^{75}Se.

The TRS plots for the lowest ($\pi=-$, $\alpha=\frac{1}{2}$) configuration in ^{75}Se are shown in the right portion of Fig. 15. At low frequencies (i.e., before the proton crossing) the equilibrium deformation of the $(-,\frac{1}{2})$ band F increases gradually from $\beta_2\sim0.30$, $\gamma\sim-11°$ ($\hbar\omega=0$) to $\beta_2\sim0.33$, $\gamma\sim-15°$ ($\hbar\omega=0.4$ MeV) — reflecting the normal centrifugal stretching of the core. For the $(-, -\frac{1}{2})$ band E the de-

formation behavior is similar. The calculations place the $\alpha=\frac{1}{2}$ Routhian below the $\alpha=-\frac{1}{2}$ signature partner, in agreement with experimental data; see Fig. 11. The signature splitting increases steadily from $\Delta e'=80$ keV at $\hbar\omega=0.2$ MeV to $\Delta e'=160$ keV at $\hbar\omega=0.4$ MeV. Slightly above $\hbar\omega=0.41$ MeV a transition towards triaxial shapes with $\gamma\sim30°$ takes place, see Fig. 15. This crossing has an origin similar to the one in the $\pi=+$, $\alpha=-\frac{1}{2}$ band, i.e., caused by the alignment of a $g_{9/2}$ proton pair. For the three-quasiparticle negative-parity band the calculations predict signature inversion; i.e., the $\alpha=-\frac{1}{2}$ Routhian E lies lower in energy than its signature partner F. This behavior is consistent with the pattern displayed in Fig. 14.

It is useful to compare the calculations with experimentally determined quantities such as transition moments to test our understanding of the microscopic structure of ^{75}Se at high spins. Clearly, since the TRS plots indicate large triaxiality for ^{75}Se, axial symmetry cannot be assumed for the direct calculation of β_2 from the quadrupole moments. The transition quadrupole moments for triaxial nuclei can be calculated [55, 56] using the expression valid in the limit of large angular momentum:

$$Q_t = (2/\sqrt{3})Q_t(\gamma = 0°)\cos(\gamma + 30°). \qquad (5)$$

The value for $Q_t(\gamma=0°)$ is given by [23, 57]

$$Q_t = \frac{6eZr_0^2A^{2/3}}{7\pi}\left\{\left[\beta_2^\rho + 7\sqrt{\pi/80}\right]^2 - \frac{49\pi}{80}\right\}, \qquad (6)$$

where $r_0=1.2$ fm. The calculated equilibrium deformation of the average field, β_2^v, must be scaled to give the resulting charge distribution deformation β_2^ρ. It has been shown [57, 58] that for the Woods-Saxon potential used in this study

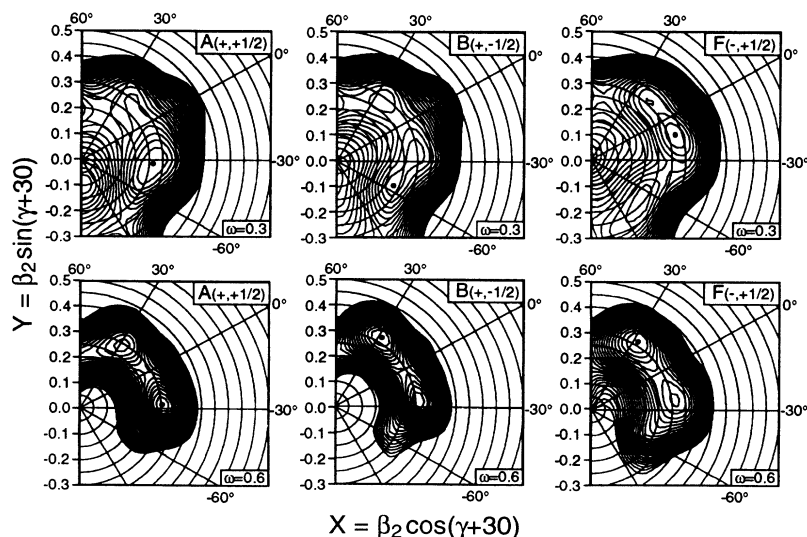$$\beta_2^\rho \approx 1.1\beta_2^v. \qquad (7)$$

FIG. 15. Total Routhian surfaces (with pairing) in the (β_2,γ) polar coordinate plane for the yrast configurations in ^{75}Se. The numbers in the boxes give the configuration labels and values of rotational frequency in MeV/$\hbar$. The distance between contour lines is 500 keV.

The results are shown in Figs. 12 and 13 along with the experimentally determined points discussed earlier. When making the comparison between experiment and theory one has to bear in mind that (i) expression (5) is valid in the limit of large angular momentum, i.e., the comparison at lowest spins is not meaningful, and (ii) band-mixing effects are ignored; i.e., the calculated curves reflect the pure geometry of the nuclear shape and the mixing amplitudes are ignored. The latter means that the calculated values should be taken as *upper* theoretical limits.

The two upper theoretical lines in Fig. 12 correspond to the more collective $g_{9/2}$ structures with $\gamma \sim -30°$. The smaller theoretical Q_t values correspond to the configurations with γ around $+20°$. The positive-parity band experimental points lie somewhat in between these two lines but seem more consistent with the more collective structure, especially in light of remark (ii) above. The 1628 and 2596 keV levels may correspond to the $\gamma = 20°$ configuration, but this could not be tested experimentally, since lifetime measurements could not be made for them.

The negative-parity band comparison is shown in Fig. 13. The upper two theoretical lines correspond to a configuration with γ around $-20°$ and the bottom two correspond to γ ranging from $+17°$ to $+42°$. Unfortunately, clear experimental evidence supporting the more collective configuration is not available since more lifetimes could not be measured. The open triangle corresponds to the 898 keV transition and the top and bottom shaded triangles correspond to the 935 and 966 keV transitions, respectively. These experimental points correspond to the frequency region of the band crossing between one-quasiparticle ($\gamma < 0$) and three-quasiparticle ($\gamma > 0$) structures and actually lie in between the theoretical predictions. It has to be mentioned that feeding corrections are expected to raise experimental Q_t values somewhat.

Table V contains the experimental values of $\widetilde{\Delta e'}$, Eq. (1), and $\Delta \widetilde{B(M1)}$, Eq. (2) extracted for the $g_{9/2}$ bands in ^{75}Se, ^{77}Kr, and ^{79}Sr. Only a limited range of spins is covered because there are substantial uncertainties involved in extrapolating the Routhians in the unfavored bands

to lower spins and in determining the signature splitting in the band crossing region at higher spins. Some lifetimes are also not known. These values can be compared with the predictions of a particle-rotor model presented by the authors of Ref. [45] as a function of a dimensionless parameter λ/κ (i.e., a normalized Fermi level). Since the calculations of Ref. [45] were carried out for a $j = \frac{11}{2}$ shell, we performed a scaling of λ/κ to the case of $j = \frac{9}{2}$ — assuming a quadratic dependence of single particle levels on Ω. Such a scaling puts the $\Omega = \frac{5}{2}$ orbital at $\lambda/\kappa = -0.25$, and the $\Omega = \frac{7}{2}$ orbital at $\lambda/\kappa = 0.5$. For neutron number $N = 41$ the single particle diagram suggests that the Fermi level lies slightly above the $[422]\frac{5}{2}$ Nilsson state; thus $\lambda/\kappa \approx 0$ is a good approximation.

The first observation that can be made is that both $\widetilde{\Delta e'}$ and $\Delta B(M1)$ are expected [45] to increase with decreasing γ from $0°$ towards $-30°$. This trend is consistent with the data: the lowest values of $\widetilde{\Delta e'}$ and $\Delta \widetilde{B(M1)}$ are found in ^{79}Sr which is expected to lie closest to the prolate axis, and the largest values are found for ^{75}Se which is predicted to be triaxial.

For ^{75}Se the values of $\widetilde{\Delta e'}$ and $\Delta \widetilde{B(M1)}$ are close to each other and are around 1.8. The closeness of $\widetilde{\Delta e'}$ and $\Delta B(M1)$ might suggest an axial shape with $\gamma \sim 0°$. However, at $\lambda/\kappa \approx 0$ the $\gamma = 0°$ diagram in Fig. 6 of Ref. [45] suggests much smaller values, around 0.2. On the other hand, their $\gamma = -25°$ diagram (Fig. 9) shows that just around $\lambda/\kappa = 0$ both ratios, Eqs. (1) and (2), are equal and are about 1.8 — in agreement with the data.

For ^{77}Kr the extracted average values of $\widetilde{\Delta e'}$ and $\Delta \widetilde{B(M1)}$ are around 1.6 and 0.8, respectively. Again, they are fairly close to the predictions by Hagemann and Hamamoto at $\gamma = -15°$ (their Fig. 8), i.e., 1.5 and 0.8. This value of γ is only slightly smaller than predicted by calculations [46].

The data for ^{79}Sr are less conclusive due to a rather large error bar for the only experimental point available. Nevertheless, one can say that the experimental result is not consistent with the purely axial shape but with small negative value of γ.

At higher spins, above the proton crossing, the $B(M1)$

TABLE V. A comparison of the signature splitting in the Routhians $\widetilde{\Delta e'}$ and in the magnetic dipole transition strengths $\Delta \widetilde{B(M1)}$. The two quantities are defined in Eqs. (1) and (2) in the text. Also listed are the values used for $\hbar\omega$ and $\Delta e'$ in Eq. (1). The former is the frequency calculated for the $I_{init} \rightarrow I_{init} - 2$ transition in the favored band. To determine the signature splitting $\Delta e'$ at this frequency, a quadratic fit was used to interpolate the Routhian in the unfavored band between nearby points. The difference between the values obtained by the quadratic and a linear interpolation was used as an estimate of the uncertainty in $\Delta e'$.

Nucleus	I_{init}	$\hbar\omega$	$\Delta e'$	$\widetilde{\Delta e'}$	$\Delta \widetilde{B(M1)}$
^{75}Se	$\frac{13}{2}^+$	0.387	0.319(19)	1.96(2)	1.70(18)
^{75}Se	$\frac{17}{2}^+$	0.480	0.324(4)	1.85(1)	1.58(13)
^{77}Kr	$\frac{13}{2}^+$	0.328	0.175(14)	1.66(7)	0.61(43)
^{77}Kr	$\frac{17}{2}^+$	0.434	0.213(6)	1.58(3)	1.09(23)
^{79}Sr	$\frac{13}{2}^+$	0.308	0.103(13)	1.20(12)	0.74(35)

rates are reduced as well as their signature splitting. Part of this reduction can be explained in terms of the shape transition towards positive values of γ. However, another factor that can be responsible for the quenching of the $B(M1)$ strength is that the three-quasiparticle bands are expected to have different deformations, at least in the frequency region directly following the proton alignment in the unfavored band.

VI. SUMMARY

The lowest positive- and negative-parity rotational bands in ^{75}Se have been studied following their production in the ^{59}Co(^{19}F,$2pn$) reaction. The bands were extended to $(\frac{29}{2}^{+})$ and $\frac{19}{2}^{-}$, and the unfavored signature $\pi = +$ band has been identified and extended to $\frac{27}{2}^{+}$. Spins were assigned or confirmed based on directional correlation ratios. Mean lifetimes for 11 states were measured using the Doppler-shift attenuation method.

A cranking model analysis revealed considerable similarity among the $N = 41$ isotones ^{75}Se, ^{77}Kr, and ^{79}Sr. A new band crossing in the $\pi = +$ band, due to the alignment of a pair of protons, has been found in ^{75}Se. The sharpness of this crossing exhibits a signature dependence similar to that seen in the other isotones, and the sharpness of the alignment increases with decreasing proton number. The cranking analysis also indicated that the data for ^{75}Se do not currently extend beyond the region of the band crossing. The onset of a band crossing was also discovered in the $\pi = -$ band, along with two other transitions which may be another band crossing or the continuation of the one-quasiparticle band.

Transition quadrupole moments extracted from lifetime measurements indicate a large deformation for ^{75}Se, with $|Q_t|$ around 2.8–2.2 e b for $\alpha = +\frac{1}{2}$. $B(M1)$ strengths were also extracted and seen to exhibit a staggering effect dependent on signature splitting. The stag-gering of $B(M1)$ strengths in ^{75}Se is similar to but larger than that for ^{77}Kr, due to a larger signature splitting in ^{75}Se.

The data were analyzed using a Woods-Saxon-Bogolyubov cranking model. The results show that at low spins the yrast structure of ^{75}Se is consistent with a triaxial shape with a deformation $\gamma \sim -30°$. The alignment of a $g_{9/2}$ proton pair triggers a shape change towards less collective triaxial configurations with $\gamma \sim 30°$. The anomalous signature splitting in the $g_{9/2}$ band is explained in terms of different deformations for the two signatures. This phenomenon is similar to the one discussed previously in ^{79}Rb [39] where *neutron* alignment causes the shape change from near-prolate to near-oblate shapes. In ^{75}Se, however, it is the $g_{9/2}$ *proton* alignment that triggers a shape change in the opposite direction, i.e., from negative to positive values of γ. At high spins the calculations predict signature inversion in both $\pi = +$ and $\pi = -$ yrast structures.

The experimental signature splitting in $B(M1)$ values and Routhians was analyzed using the method suggested by Hagemann and Hamamoto [45]. The data suggest tri-axial deformations for ^{75}Se and they are consistent with a transition towards prolate shapes with increased proton number.

ACKNOWLEDGMENTS

[1] J.H. Hamilton, *Heavy Ion Collision*, Lecture Notes in Physics Vol. 168, edited by G. Madurga and M. Lozano (Springer-Verlag, Berlin, 1982), p. 631.

[2] J.H. Hamilton, in *Treatise on Heavy Ion Science*, edited by D.A. Bromley (Plenum, New York, 1989), Vol. 8, p. 1.

[3] S. Åberg, H. Flocard, and W. Nazarewicz, Annu. Rev. Nucl. Part. Sci. **40**, 439 (1990).

[4] W. Nazarewicz, in *High Spin Physics and Gamma-soft Nuclei*, edited by J.X. Saladin, R.A. Sorensen, and C.M. Vincent (World Scientific, Singapore, 1991), p. 406.

[5] M. Wiosna, J. Busch, J. Eberth, M. Liebchen, T. My-laeus, N. Schmal, R. Sefzig, S. Skoda, and W. Teichert, Phys. Lett. B **200**, 255 (1988).

[6] F. Seiffert, W. Lieberz, K.P. Schmittgen, R. Reinhardt, R. Wirowski, R. Wrzal, K.O. Zell, P. von Brentano, R. Schwenger, and L. Funke, Z. Phys. A **336**, 241 (1990).

[7] M.S. Kaplan, J.X. Saladin, D.F. Winchell, H. Takai, and J. Dudek, Phys. Rev. C **44**, 668 (1991).

[8] K.O. Zell, H.-G. Friederichs, B. Heits, D. Hippe, H.W. Schuh, P. von Brentano, and C. Protop, Z. Phys. A **276**, 371 (1976).

[9] K.O. Zell, W. Gast, D. Hippe, H.W. Schuh, and P. von Brentano, Z. Phys. A **292**, 135 (1979).

[10] T. Mylaeus, J. Busch, J. Eberth, M. Liebchen, R. Sefzig, S. Skoda, W. Teichert, M. Wiosna, P. von Brentano, K. Schiffer, K.O. Zell, A.V. Ramayya, and W. Nazarewicz, J. Phys. G **15**, L135 (1989).

[11] C.J. Gross, P.D. Cottle, D.M. Headly, U.J. Hüttmeier, E.F. Moore, and S.L. Tabor, Phys. Rev. C **36**, 2127 (1987).

[12] P.D. Cottle, J.W. Holcomb, T.D. Johnson, K.A. Stuckey, S.L. Tabor, P.C. Womble, S.G. Buccino, and F.E. Durham, Phys. Rev. C **42**, 1254 (1990).

[13] L.C. Aamodt and P.C. Fletcher, Phys. Rev. **98**, 1224 (1955).

[14] Inge-Maria Ladenbauer-Bellis and H. Bakhru, Phys. Rev. **178**, 2019 (1969).

[15] E. Finckh, U. Jahnke, B. Schreiber, and A. Weidinger, Nucl. Phys. **A144**, 67 (1970).

[16] A. Coban, J.C. Willmott, J.C. Lisle, and G. Murray, Nucl. Phys. **A182**, 385 (1972).

[17] N.E. Sanderson, Nucl. Phys. **A216**, 173 (1973).

[18] N.E. Sanderson and R.G. Summers-Gill, Nucl. Phys. **A261**, 93 (1976).

[19] K.O. Zell, H.-G. Friederichs, B. Heits, P. von Brentano, and C. Protop, Z. Phys. A **272**, 27 (1975).

[20] Y.K. Agarwal, S.M. Bharathi, S.K. Bhattacherjee, B. Lal, B. Sahai, and C.V.K. Baba, in *Electromagnetic Properties of Low Lying Levels in* ^{75}*Se*, Proceedings of the International Conference, München, 1973, edited by J. DeBoer and H.J. Mang (North-Holland, Amsterdam, 1973), p. 288.

[21] Y. Tokunaga, H. Sayfarth, O.W.B. Schult, S. Brant, V. Paar, D. Vretenar, H.G. Borner, G. Barreau, H. Faust, Ch. Hofmeyr, and K. Schreckenbach, Nucl. Phys. **A430**, 269 (1984).

[22] G.P.S. Sahota, V.K. Mittal, S.D. Sharma, H.S. Sahota, G. Singh, S.S. Datta, and I.M. Govel, Phys. Rev. C **44**, 987 (1991).

[23] E.F. Moore, P.D. Cottle, C.J. Gross, D.M. Headly, U.J. Hüttmeier, S.L. Tabor, and W. Nazarewicz, Phys. Rev. C **38**, 696 (1988).

[24] L.C. Northcliffe and R.F. Schilling, Nucl. Data Sec. A **7**, 233 (1970).

[25] J.F. Ziegler and W.K. Chu, At. Data Nucl. Data Tables **13**, 463 (1974).

[26] S. Kalbitzer, H. Oetzmann, N. Grahmann, and A. Feverstein, Z. Phys. A **278**, 223 (1976).

[27] J. Lindhard, M. Scharff, and H.E. Schiott, K. Dan. Vidensk. Selsk., Mat.-Fys. Medd. **33**, No. 14 (1963).

[28] A.E. Blaugrund, Nucl. Phys. **88**, 501 (1966).

[29] A. Gravon, Phys. Rev. C **21**, 230 (1980).

[30] F. Seiffert, R. Schwenger, G. Winter, L. Funke, W. Lieberz, R. Reinhardt, K.P. Schmittgen, D. Weil, R. Wrzal, K.O. Zell, and P. von Brentano, Z. Phys. A **340**, 141 (1991).

[31] S. Frauendorf and F. R. May, Phys. Lett. **125B**, 245 (1983).

[32] G. Winter, J. Döring, L. Funke, H. Prade, H. Rotter, R. Schwengner, A. Johnson, and A. Nilsson, J. Phys. G **14**, L13 (1988).

[33] R. Schwengner, J. Döring, L. Funke, G. Winter, A. Johnson, and W. Nazarewicz, Nucl. Phys. **A509**, 550 (1990).

[34] L. Funke, F. Dönau, J. Döring, P. Kemnitz, E. Will, G. Winter, L. Hildingson, A. Johnson, and Th. Lindblad, Phys. Lett. **120B**, 301 (1983).

[35] Ö. Skeppstedt, C.J. Lister, A.A. Chishti, B.J. Varley, W. Gelletly, U. Lenz, R. Moscrop, and L. Goettig, Nucl. Phys. **A511**, 137 (1990).

[36] S.L. Tabor, P.D. Cottle, C.J. Gross, U.J. Hüttmeier, E.F. Moore, and W. Nazarewicz, Phys. Rev. C **39**, 1359 (1989).

[37] C.J. Lister, B.J. Varley, W. Fieber, J. Heese, K.P. Lieb, F.K. Warburton, and J.W. Olness, Z. Phys. A **329**, 413 (1988).

[38] U.J. Hüttmeier, C.J. Gross, D.M. Headly, E.F. Moore, S.L. Tabor, T.M. Cormier, P.M. Stwertka, and W. Nazarewicz, Phys. Rev. C **37**, 118 (1988).

[39] R. Bengtsson, W. Nazarewicz, Ö Skeppstedt, and R. Wyss, Nucl. Phys. **A528**, 215 (1991).

[40] R. Bengtsson and W. Nazarewicz, in Proceedings of the XIX Winter School on Physics, Zakopane, 1984, edited by Z. Stachura, Report IFJ No. 1268, p. 171.

[41] S.L. Tabor, Phys. Rev. C **34**, 311 (1986).

[42] R. Bengtsson, in *Nuclear Structure of the Zirconium Region*, edited by J. Eberth, R.A. Meyer, and K. Sistemich (Springer-Verlag, Berlin, 1988), p. 371.

[43] I. Hamamoto and H. Sagawa, Nucl. Phys. **A327**, 99 (1979).

[44] I. Hamamoto, Phys. Lett. **106B**, 281 (1981).

[45] G.B. Hagemann and I. Hamamoto, Phys. Rev. C **40**, 2862 (1989).

[46] C.J. Gross, P.D. Cottle, D.M. Headly, U.J. Hüttmeier, E.F. Moore, S.L. Tabor, and W. Nazarewicz, Phys. Rev. C **36**, 2601 (1987).

[47] T.D. Johnson, J.W. Holcomb, P.C. Womble, P.D. Cottle, S.L. Tabor, F.E. Durham, S.G. Buccino, and M. Matsuzaki, Phys. Rev. C **42**, 2418 (1990).

[48] J. Heese, K.P. Lieb, S. Ulbig, B. Wormann, J. Billowes, A.A. Chishti, W. Gelletly, C.J. Lister, and B.J. Varley, Phys. Rev. C **41**, 603 (1990).

[49] F. Dönau, Nucl. Phys. **A471**, 469 (1987).

[50] M. Matsuzaki, Phys. Rev. C **39**, 691 (1989).

[51] W. Nazarewicz, J. Dudek, R. Bengtsson, T. Bengtsson, and I. Ragnarsson, Nucl. Phys. **A435**, 397 (1985).

[52] W. Nazarewicz and T. Werner, in [42], p. 277.

[53] A.A. Chishti, W. Gelletly, C.J. Lister, B.J. Varley, and Ö. Skeppstedt, J. Phys. G **16**, 481 (1990).

[54] C.J. Gross, J. Heese, K.P. Lieb, S. Ulbig, W. Nazarewicz, C.J. Lister, B.J. Varley, J. Billowes, A.A. Chishti, J.H. McNeill, and W. Gelletly, Nucl. Phys. **A501**, 367 (1989).

[55] P. Ring, A. Hayashi, K. Hara, H. Emling, and E. Grosse, Phys. Lett. **110B**, 423 (1982).

[56] I. Hamamoto and B.R. Mottelson, Phys. Lett. **132B**, 7 (1983).

[57] W. Nazarewicz, M.A. Riley, and J.D. Garrett, Nucl. Phys. **A512**, 61 (1990).

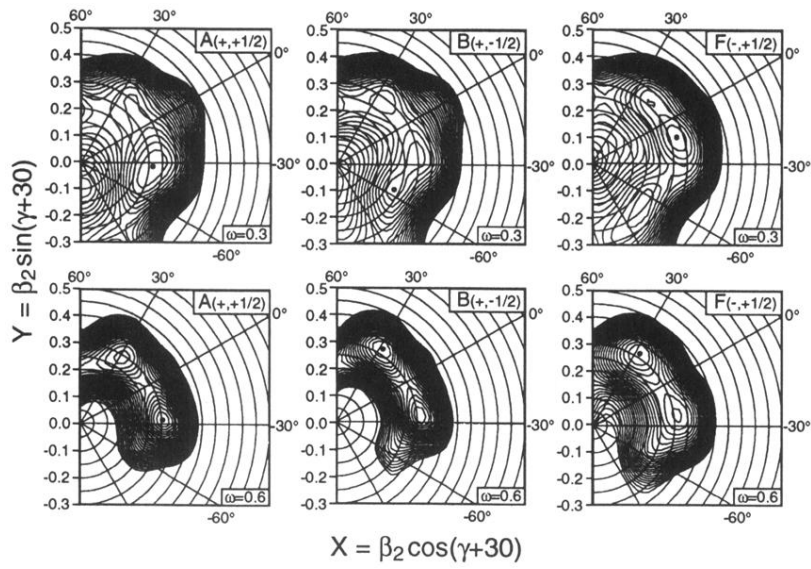[58] J. Dudek, W. Nazarewicz, and P. Olanders, Nucl. Phys. **A420**, 285 (1984).

FIG. 15. Total Routhian surfaces (with pairing) in the (β_2, γ) polar coordinate plane for the yrast configurations in ^{75}Se. The numbers in the boxes give the configuration labels and values of rotational frequency in MeV/$\hbar$. The distance between contour lines is 500 keV.